Journal of Materials Science and Chemical Engineering, 2022, 10, 1-15
https://www.scirp.org/journal/msce
ISSN Online: 2327-6053
ISSN Print: 2327-6045

Property Analysis of SiC-Crystals Grafted with Graphene Using Molecular Dynamics Simulations

Taraneh Lewtschenko, Maya Pagel, Niklas Wenzel, Christina Oligschleger

Department of Applied Science, Bonn-Rhein-Sieg University of Applied Sciences, Rheinbach, Germany
Email: christina.oligschleger@h-brs.de

How to cite this paper: Lewtschenko, T., Pagel, M., Wenzel, N. and Oligschleger, C. (2022) Property Analysis of SiC-Crystals Grafted with Graphene Using Molecular Dynamics Simulations. *Journal of Materials Science and Chemical Engineering*, **10**, 1-15.
https://doi.org/10.4236/msce.2022.1011001

Received: October 3, 2022
Accepted: November 7, 2022
Published: November 10, 2022

Abstract

Silicon carbide and graphene possess extraordinary chemical and physical properties. Here, these different systems are linked and the changes in structural and dynamic properties are investigated. For the simulations performed a classical molecular dynamic (MD) approach was used. In this approach, a graphene layer (N = 240 atoms) was grafted at different distances on top of a 6H-SiC structure (N = 2400 atoms) and onto a 3C-SiC structure (N = 1728 atoms). The distances between the graphene and the 6H are 1.0, 1.3 and 1.5 Å and the distances between the graphene layer and the 3C-SiC are 2.0, 2.3, and 2.5 Å. Each system has been equilibrated at room temperature until no further relaxation was observed. The 6H-SiC structure in combination with graphene proves to be more stable compared to the combination with 3C-SiC. This can be seen well in the determined energies. Pair distribution functions were influenced slightly by the graphene layer due to steric and energetic changes. This becomes clear from the small shifts of the C-C distances. Interactions as well as bonds between graphene and SiC lead to the fact that small shoulders of the high-frequency SiC-peaks are visible in the spectra and at the same time the high-frequency peaks of graphene are completely absent.

Keywords

Molecular Dynamics, Silicon Carbides, Graphene, Nano-Systems

1. Introduction

Silicon carbides (SiC) play a crucial role in the synthesis of ceramics due to their properties, e.g., high hardness, low thermal expansion and good thermal conductivity. Heat-shock resistance is particularly interesting for applications of ceramics, e.g., in turbines. Another important field of application for SiC is its use

in the field of semiconductor technology. Here, the electronic properties associated with the band gap come into play. Inherently an insulator, SiC can be used as a semiconductor in electronic devices, e.g., as a p-type semiconductor by doping with Al-ions.

Different stacking sequences of the geometrically defined spherical layers form different SiC polytypes. The spherical layers of the SiC are so-called bilayers, which consist of a Si-atomic layer and a C-atomic layer. The structures of SiC occur in 3 different symmetries. The hexagonal and rhombohedral modification is called α-SiC, the cubic modification is referred to as β-SiC. According to the nomenclature of Ramsdell, the structure of the SiC structure can be described in more detail [1]. First, the number of double layers in a unit cell is denoted, followed by a letter standing for the crystalline symmetry. The letters are C for cubic, H for hexagonal and R for rhombohedral symmetries. Consequently, a polytype with hexagonal symmetry and an elementary cell, consisting of two double layers, is called 2H-SiC. Cubic β-SiC undergoes a conversion into the α-SiC at approx. 2100˚C, usually in the 6H, 4H and 15R structures, which is why the β-SiC is called low-temperature modification and the α-SiC is called a high-temperature modification, resp.

In our studies we pay special attention to the 6H- and 3C-SiC modifications. The 6H-modification has an energy gap of 3.0 eV [2], a carrier mobility of approximately 3.0 cm^{-3}/Vs and a carrier concentration (10^{-5} cm^{-3}) that is significantly lower than the one of 3C-SiC [3]. Common synthesis routes include electrochemical etching [4], chemical vapour deposition [5], direct carbonisation [6] or carbothermal reduction [7]. Even though silicon carbides generally can be found in a very broad range of application, not so much is known about uses of hexagonal SiC specifically. While it for example exhibits comparably unsatisfactory performance in experimental work regarding photoluminescence [8], it shows useful effects as a composite component [6] and is one of the potential candidates with the prospect of realising optical switching in the visible range due to its wide band gap [9].

Compared to the 6H-SiC, the smaller band gap of 2.3 eV and higher symmetry of the 3C-SiC offer a larger bulk and channel electron mobility and increased intrinsic concentration of charge carriers. 3C-SiC films exhibit a zinc-blende crystal structure and can be grown on Si substrates, which is low cost and provides high flexibility in increasing lateral dimensions. The low cost of the 3C-SiC approach and the high scalability to Si wafers of more than 300 mm make this technology very popular for applications in hybrid electric vehicles, air conditioning and LED lighting system [10]. Much research is being done in the synthesis and characterisation of 3C-SiC nanowires, nanoflakes or nanowhiskers.

On top of that, graphene will also play an important role in our studies. Graphene is made of carbon atoms arranged in a hexagonal pattern, forming a two-dimensional honeycomb-like structure. This means that graphene is a single layer of graphite, with the atoms having a bonding angle of 120˚ and a C-C

bonding distance equivalent to 1.42 Å [11].

Graphene exhibits exceptional electrical and thermal conductivity, has a very high specific surface area and shows remarkable mechanical properties [12] [13]. These properties make graphene attractive for a wide range of applications. Graphene can be used as an electrode material (e.g. in batteries, sensors or fuel cells), in ultra-thin membranes for water treatment, as a transistor, in composites or even for graphene sensors [11] [12]. While many possible production routes can be used to produce graphene, chemical vapour deposition is most frequently used in order to have high-quality graphene and good control over the production of the layers [13] [14] [15].

In this work, molecular dynamics simulations are used to heat and equilibrate both SiC structures and graphene to room temperature. Subsequently, the configurations are attached to each other at small distances. The influence of the different chosen distances between the SiC crystals and the graphene layer on structural and dynamic properties is investigated.

2. Methods

For the simulations a classical molecular dynamics approach which is a state of the art method for more than three decades [16] [17] [18] [19] was used. Still, this approach has recently been applied in studies of different effects in combined structures, either for studying mechanical behaviour [20] [21], thermal properties [22], or fabrication and synthesis processes [23] [24]. Nevertheless, one should have in mind that in nano-systems the physics are governed and dominated by quantum effects which are not considered in this type of simulation. By using the numerical integration of the Newtonian equation of motion as the mathematical basis of this simulation, electronic contributions are neglected and only atomic/vibronic behaviour is taken into account. However, since the system sizes which we consider exceed 1000 atoms, our simulations could not easily be transferred to quantum-mechanical calculations, though these would be helpful.

We studied 6H-SiC-systems comprising a total number of $N = 2400$ atoms, 3C-SiC-system with $N = 1728$ atoms and a graphene layer of $N = 240$ carbon-atoms. The MD integration time step is about $\Delta t = 0.47402$ fs. For our work, periodic boundary conditions were used in the MD analysis. This means stratifications were created for top and bottom so that there is no fluctuation up and down. Graphene and 6H/ 3C-SiC were layered on top of each other at different distances. The distances between the graphene and the 6H were 1.0, 1.3 and 1.5 Å and between the graphene and the 3C-SiC with a larger distance were 2.0, 2.3 and 2.5 Å at a pressure of 0 bar. The temperature was raised from 8 K to 290 K and then equilibrated at room temperature. The equilibration phase took place in 5000 molecular dynamic steps (MDS). Each system was equilibrated until the energy fluctuations were noise and no relaxation was observed. This means that no spatial rearrangements or energetic optimisations were found. Usually up to 5 runs were necessary until no more relaxation was observed. In

order to make a statement about the effects on the properties of the combinations of graphene with the SiC polytypes at different distances, the output files are compared with respect to their energy distributions, their pair distributions and the frequency spectra at the different distances.

2.1. Potential

For the simulations of the carbon structures we use a potential which was developed to describe graphite or diamond structures as well as hydrocarbon molecules. This potential was proposed and adapted by D. W. Brenner [25]. This empirical potential is well suited to reproduce structural properties and dynamic characteristics of a variety of Si-C-H systems. In individual cases, optimizations of the potential parameters can be made, for example, to better describe phonons in graphene. Since a combination of different systems is studied, we use the Brenner potential described here. The binding energy E_b is given by a potential consisting of two-body terms (considering short-range interactions of attractive and repulsive nature).

$$E = \sum_i \sum_{j>i} V_R\left(r_{ij}\right) - \bar{B}_{ij} V_A\left(r_{ij}\right) \tag{1}$$

Here is $V_R\left(r_{ij}\right)$ the repulsive and $V_A\left(r_{ij}\right)$ the attractive part of the potential. The averaged bonding situation for the atoms i and j is described with the last factor $\bar{B}_{ij}$. The detailed functional equations are shown as follows:

$$\begin{aligned} V_R\left(r_{ij}\right) &= f\left(r_{ij}\right) \frac{c_{ij}}{s_{ij}-1} \mathrm{e}^{-\sqrt{2s_{ij}}\beta_{ij}\left(r_{ij}-r_{ij,0}\right)} \\ V_A\left(r_{ij}\right) &= f\left(r_{ij}\right) \frac{c_{ij}}{s_{ij}-1} s_{ij} \mathrm{e}^{-\sqrt{\frac{2}{s_{ij}}}\beta_{ij}\left(r_{ij}-r_{ij,0}\right)} \\ \bar{B}_{ij} &= \left(B_{ij}+B_{ji}\right)/2 + F\left(N_i^t, N_j^t, N_{ij}^{conj}\right)/2 \end{aligned} \tag{2}$$

The form of the potential with the parameters $c_{ij}, s_{ij}, \beta_{ij}$ and r_{ij} is of the same type as a Morse potential. These parameters represent type-specific properties (energies, length scales). The function $f\left(r_{ij}\right)$ has only a short interaction range and is defined by:

$$f(r) = \begin{cases} 1 & \text{for } r < r_{ij,1} \\ \frac{1}{2}\left(1+\cos\left(\pi \frac{r-r_{ij,1}}{r_{ij,2}-r_{ij,1}}\right)\right) & \text{for } r_{ij,1} \le r < r_{ij,2} \\ 0 & \text{for } r \ge r_{ij,2} \end{cases} \tag{3}$$

By applying periodic boundary conditions, we want to reduce surface effects generated due to the size of the system. For this purpose, the initial volume is kept constant during the simulation and the virial of the configuration is monitored to consider the internal pressure [26].

2.2. Observables

A quantifiable parameter is needed to determine the stability of the configura-

tions or rather the structural changes. For this purpose, we use the distance between the initial reference phase and the aged ensembles as a quantifiable parameter. The atomic shifts are measured by using the squared displacements:

$$\Delta R^2 = \sum_n \left(\boldsymbol{R}_n^i - \boldsymbol{R}_n \right)^2 \tag{4}$$

The parameter $\boldsymbol{R}_n^i$ refers to the position vector of the atom n depending on its position in the configuration i of the potential energy surface and $\boldsymbol{R}_n$ to the position of the atom n in the reference system. The total displacement R (RSD) which is responsible for a structural change is measured in Å and is determined by the following equation $R = \sqrt{\Delta R^2}$.

The velocities of the atoms can be used to determine the temperatures in the simulations. To keep the temperature in canonical simulations (NVT-ensemble) constant, the velocities of the atoms are rescaled every 100 time steps.

Furthermore we determine the partial pair-correlation functions $g(r)$ a structural property which exhibits the status of matter:

$$g(r) = \left\langle \frac{n(r)}{4\pi r^2 \rho \Delta r} \right\rangle \tag{5}$$

With $n(r)$ being the number of atoms at a distance r in a sphere with thickness Δr. This sphere is located around a reference atom, ρ is the number density of the atoms in the systems and $\langle\,\rangle$ stands for the averaging over configurations which are calculated throughout the MD simulations. We calculate correlations of pairs of atoms i and j, *i.e.* Si-Si, Si-C and C-C pairs, resp.

The velocity-autocorrelation function (VACF) can be used to find typical fluctuations of the structures, which can be used to identify underlying vibrations.

$$f_v(t) = \frac{\left\langle \sum_{i=1}^{N} \boldsymbol{v}_i(0) \boldsymbol{v}_i(t) \right\rangle}{\left\langle \sum_{i=1}^{N} \boldsymbol{v}_i(0) \boldsymbol{v}_i(0) \right\rangle} \tag{6}$$

By using a cosine-transformation on the velocity-autocorrelation function, we obtain the vibration density of states (DOS):

$$Z(\nu) = \frac{1}{Z_0} \int_0^{t_{obs}} \cos(2\pi\nu t) \exp\left(-\lambda t^2\right) f_v(t) \mathrm{d}t \tag{7}$$

λ is a damping factor that broadens the δ peaks in the frequency spectrum [27] [28]. t_{obs} is the observation time for the velocity-autocorrelation function and Z_0 a normalisation constant. [26] The frequencies that can be detected in the MD simulations depend on the observation period t_{obs}. Basically, the longer the observation period, the lower is the frequency of oscillations that can be detected in the system.

3. Results and Discussion

The change of energy in the combined structures is used to monitor the process of equilibration. In **Figure 1** the energy (given in eV) is shown exemplary for the

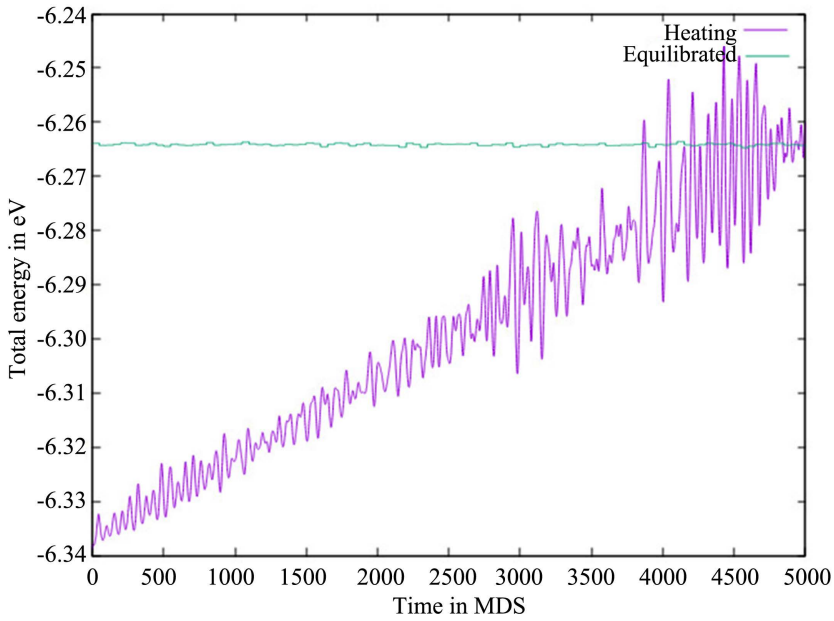

Figure 1. Energy of the hexagonal SiC-crystal during heating and after equilibration.

6H-SiC structure and is plotted against time in MD steps. The purple curve shows the initial heating phase of the material and the green curve shows the equilibrated energy after multiple MD runs. The heating curve increases linearly and settles at the value −6.26 eV after around 4500 MDS. After settling, the fluctuation is still very strong. At the end of the equilibration period of 40,000 MD steps the equilibrated curve shows a constant energy of −6.265 eV without strong fluctuation. This process was also performed for 3C-SiC and graphene. After the respective equilibration phases, SiC and graphene structures with different distances have been assembled. Visual examples of those crystal structures and graphene layers can be found in **Figure 2**.

For the equilibrated structures we measured the mean values and standard deviations of energies, pressures and atomic displacements depending on the distances between the graphene layer and the SiC-bulk structures. The averages are calculated over the last 5000 molecular dynamic steps of the equilibration period. In **Table 1** we show the findings for the 6H-SiC-graphene and 3C-SiC-graphene systems, resp.

The temperatures fluctuate in the range of 1% to 1.5% for the equilibrated systems. Potential and total energies exhibit deviations less than 0.005%, which is a clear hint for well equilibrated structures. According to energies per atom (both potential and total energy) the 6H-SiC-graphene with a distance of 1.0 Å is the most stable structural entity. Here we observe the creation of additional bonds between the C-atoms of the graphene layer and the C-atoms of the surface of the 6H-SiC-structure. With increasing distance between the graphene layer and the surface of the 6H-SiC the number of bindings is reduced and therefore the energetic stability of the systems decreases. Since the pressure comprises both kinetic and potential energy per volume, *i.e.* the first contribution is

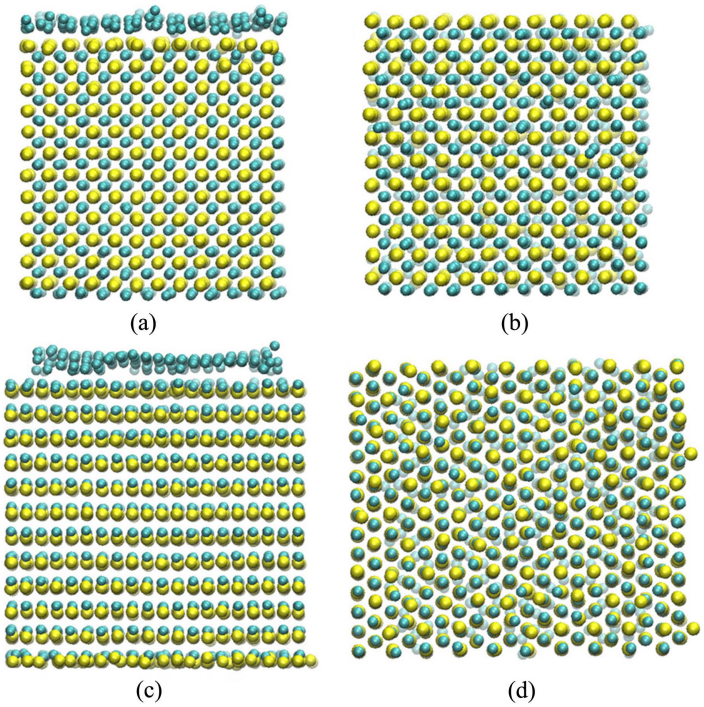

Figure 2. Exemplary structures of SiC-crystals grafted with graphene. C-atoms are colored blue, Si-atoms are yellow. (a): Side view of equilibrated 3C-SiC with graphene layer (distance 2.1 Å). (b): Bottom view of equilibrated 3C-SiC with graphene layer (distance 2.1 Å). The cubic structure can be identified easily. (c): Side view of equilibrated 6H-SiC with graphene layer (distance 1.0 Å). (d): Bottom view of equilibrated 6H-SiC with graphene layer (distance 1.0 Å). The hexagonal structure can be identified easily.

Table 1. Comparison of energies (temperature, potential and total energies), pressures and distances (RSD) given as mean value ± standard deviation of the different distances between SiC-systems and graphene.

Observables	6H-SiC-graphene			3C-SiC-graphene		
	1.0Å	1.3Å	1.5Å	2.1Å	2.3Å	2.5Å
Temperature K	298.06 ± 3.62	298.03 ± 3.58	298.03 ± 3.52	297.99 ± 3.90	298.05 ± 4.20	298.11 ± 4.24
Potential energy eV	−6.2414 ± 0.0004	−6.2398 ± 0.0005	−6.2204 ± 0.0004	−6.2179 ± 0.0005	−6.2205 ± 0.0005	−6.2194 ± 0.0005
Total energy eV	−6.2031 ± 0.0002	−6.2014 ± 0.0002	−6.1821 ± 0.0002	−6.1821 ± 0.0003	−6.1822 ± 0.0003	−6.1811 ± 0.0003
Pressure GPa	−11.397 ± 0.110	−11.073 ± 0.132	−9.937 ± 0.111	−11.388 ± 0.223	−11.484 ± 0.216	−11.208 ± 0.196
RSD Å	8.8278 ± 0.6516	8.7578 ± 0.6685	10.4239 ± 0.9430	7.4831 ± 0.5632	7.5236 ± 0.5797	8.4160 ± 0.7692

proportional to temperature and the latter one to potential energy, its fluctuations are governed mainly by the deviations, which we observe in temperature. Therefore, we find pressure deviations in the range of 1% to 2%. The values of the RSD, *i.e.* the total displacement of all atoms in the corresponding systems, vary from 8.8 Å to 10.4 Å in the 6H-SiC-graphene structures and from 7.5 Å to 8.4 Å in the 3C-SiC-graphene structures, resp. In the 6H-SiC-graphene configuration we have roughly 34% more atoms than the 3C-SiC-graphene structure. However, the total displacements in the 6H-SiC-graphene systems are relatively low compared to the 3C-SiC-graphene. This can be explained with a higher bonding situation, in which the flexibility of the additionally connected atoms is reduced.

3.1. Pair Distribution

Mutual influences of the combined structures can be seen in changes of the pair distribution functions compared to the individual ones. In our systems we have three types of pair distribution functions, because we have three pairs of atoms, *i.e.* Si-C, C-C and Si-Si, resp. As long as Si-atoms are involved we observe only slight changes of peak-heights and widths, which are nearly independent on the distance between the graphene layer and the SiC-systems. Especially the peak positions in the Si-C or Si-Si pair distributions are not affected. Since we do not notice strong changes in the pair distribution as long as Silicon-atoms are involved, we focus here on the C-C pair distributions.

In Figure 3 the C-C pair distribution functions for the 3C-SiC structures are shown. The most prominent peak at a distance of approximately $d = 3.1$ Å is present in the pure 3C-SiC crystal (black line) and can also be found in all other graphene-combined structures. It represents the smallest distance between two C-atoms and correlates well with experimental data found in literature [29]. The correlation between pure SiC peaks and graphene-combined SiC peaks continues

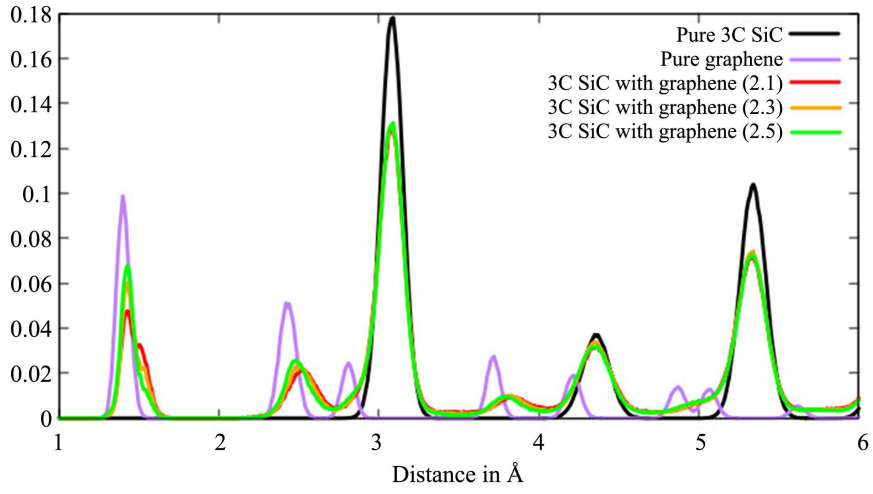

Figure 3. C-C pair distribution function for 3C-SiC. All results come from equilibrated structures. For the 3C-SiC structures with graphene the value in brackets refers to the distance between the 3C-SiC crystal and the applied graphene layer in Ångström.

throughout the entire pair distribution function and can be found at $d \approx 4.4$ Å and $d \approx 5.3$ Å. Here, a definite difference in peak height between the different graphene distances (red, yellow, green) cannot be found. This means that the distance between the graphene layer and SiC crystal did not strongly interfere with the C-C distances in the SiC crystal.

The pure graphene (purple line) is very different from the pure 3C-SiC pair distribution function. Carbon atoms show much smaller distances starting at the smallest distance at 1.4 Å with its most prominent peak. Peak height generally decreases with increasing C-C distance after that. Again, the C-C pair distribution function for pure graphene correlates well with results found in literature [30]. At the distances where peaks appear in the pure graphene peaks may also appear in the graphene-combined structures. This is especially notable at the prominent peak at 1.4 Å where definite peaks can be seen in the SiC-structures combined with graphene. At this point, an influence of the distance between the SiC and graphene layer can be found. The peak height decreases with decreasing distance of the graphene layer. Also, a small shift can be noted. This shows that the degree of interaction of SiC and graphene decreases with increasing distance. Depending on the distance, different levels of energy and attracting forces are prominent. Differences in peak shape can therefore either have steric (due to different hybridisation states) or energetic reasons. Furthermore, an appearance of shoulders in the peaks can be noted. The shoulder is most prominent in the structure with the smallest distance between SiC and graphene, again implicating that there the degree of interaction is highest, possibly leading to shifts in the atomic structure due to a transition between hybridisation states. The influence of the pure graphene peaks on the combined structures decreases with distance. There, the pair distribution functions only show vague peaks or slight bumps (note e.g. at Å ≈ 5).

In **Figure 4** the pair distribution functions for the 6H-SiC structures are shown. The pure 6H-SiC is very similar to the pure 3C-SiC in **Figure 3**. The only

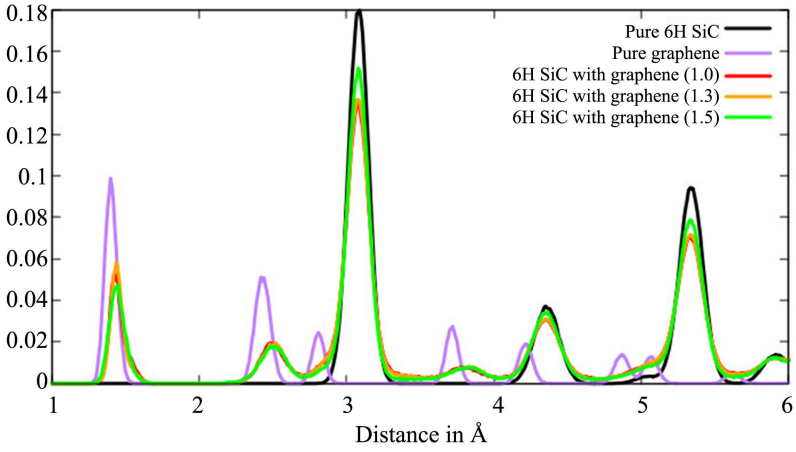

Figure 4. C-C pair distribution function for 6H-SiC. All results come from equilibrated structures. For the 6H-SiC structures with graphene the value in brackets refers to the distance between the 6H-SiC crystal and the applied graphene layer in Ångström.

notable differences are the small bump at 5.05 Å and the small peak at 5.9 Å that are only present in the 6H-SiC as well as the decreased peak height for the 6H-SiC at the 5.3 Å-peak. The pure graphene remains unchanged.

Different to the 3C-SiC structure, here we see that the peak height at the pure SiC-peaks (Å = 3.1, 4.4 and 5.3) is highest in the combined structure with the highest distance between graphene and SiC (green line). It decreases with decreasing graphene layer distance. This tendency cannot be seen at the small distances at the graphene-peaks. There, the middle distance (Å = 1.3, yellow line) shows the highest peak. A definite difference in peak height at higher C-C distances cannot be found.

3.2. Frequency Spectra

In addition to a focus on structural changes, we also consider the dynamics of the systems. For this we examined the density of states $Z(\nu)$ of the individual and the combined systems, resp.

Figure 5 shows the spectrum with frequencies in the THz range for the 3C-SiC structures. The here investigated data is related to the bonds between the C-atoms of the graphene layer and the C-atoms of the surface of the 3C-SiC structure. At the beginning, it is directly visible that the curves for the pure SiC as well as the three curves for the combined structures with graphene follow a similar curve progression. But stronger fluctuations can be seen from time to time, especially in relation to the pure SiC (black curve). This is shown by the fact that the curve of the pure 3C-SiC often varies somewhat upwards or downwards from the curves of the combined structures with graphene. At approximately 3 to 9 THz and around 14.5 THz, only minor peaks can be seen. The peak in the range from around 3 to 9 THz is much broader than the peak at approximately 14.5 THz. Further in the high-frequency range at about 22 to 25

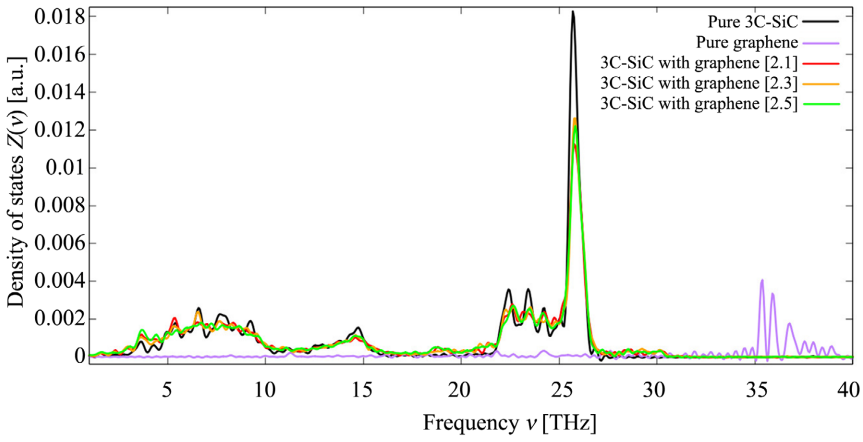

Figure 5. The spectrum of 3C-SiC for all equilibrated results, with the vibrational density of the states $Z(\nu)$ in arbitrary units plotted against the frequency ν in THz. The red/orange/green curves show the 3C-SiC structures which are grafted with graphene. The brackets contain the value in Ångström for the distance between the 3C-SiC crystal and the graphene layer.

THz, smaller peaks can be found. They are followed by another large peak at about 25.7 THz, which shows this time clear differences in the intensity of the curves. The black curve of the pure 3C-SiC is somewhat more prominent and differs slightly upwards from the curves of the combined structures with graphene (red/orange/green curves). Then the large peaks drop down quickly and no more peaks can be observed.

Also, the influence of the different distances of the graphene layer from the SiC crystal only can be seen clearly at the larger peaks in the high-frequency range of the spectrum near 25.7 THz. In fact, the bigger the distance of the graphene layer from the 3C-SiC crystal, the fewer bonds are formed between them. So, if the entire spectrum is considered, it can be said that the peak height also decreases with the decreasing distance of the graphene layer and an increasing number of bonds. Nonetheless, there are also deviations from that, especially where larger fluctuations appear in the curves. For example, at the larger peak in the spectrum, at about 25.7 THz, a slightly higher intensity can be seen for the distance of 2.3 Å than for the distance of 2.5 Å. However, this can also be seen for the minor peaks at about 5.5 and 6.5 THz.

In contrast, the purple curve for the pure graphene shows a completely different behaviour. The curve shows practically no significant fluctuations up to approximately 33 THz. Only in the high-frequency range above 33 THz smaller peaks can be seen, which lead to somewhat higher intensities around 35 - 37 THz, but then drop down again very quickly and are no longer present at frequencies around 40 THz. This shows that the influence of the graphene layer on the combined structures is rather small, which can be explained quite simply by the smaller number of atoms in the graphene layer compared to the 3C-SiC crystal or those due to additional bonding the high-frequency peaks have completely been overdamped and are not longer existent in the combined structure.

In **Figure 6**, the spectrum with the frequencies for the 6H-SiC structures is shown. In this case, the C-C bonds of the graphene layer and the surface of the

6H-SiC structure are considered. Compared to the 3C-SiC structure, the 6H-SiC structure shows hardly any differences in the curve. The minor peaks are found again at around 3 to 9 THz and about 14.5 THz. Further in the high-frequency range at about 22 to 25 THz, the smaller peaks are present as well, followed by the higher peak at approximately 25.7 THz. The intensity of the larger peak is somewhat higher for the 6H structures than for the 3C structures. At this position in the spectrum, the influence of the different distances of the graphene layer from the SiC crystal becomes even more obvious (red/orange/green curve). In comparison to the 3C-SiC structure, it can be seen here clearly that the peak height decreases with the decreasing distance of the graphene layer and the increasing number of bonds.

A general observation regarding the 6H-SiC structures is that there are almost no fluctuations in the curves and they overlap more than the 3C-SiC structures. This can be explained by the fact that, according to the potential energies and

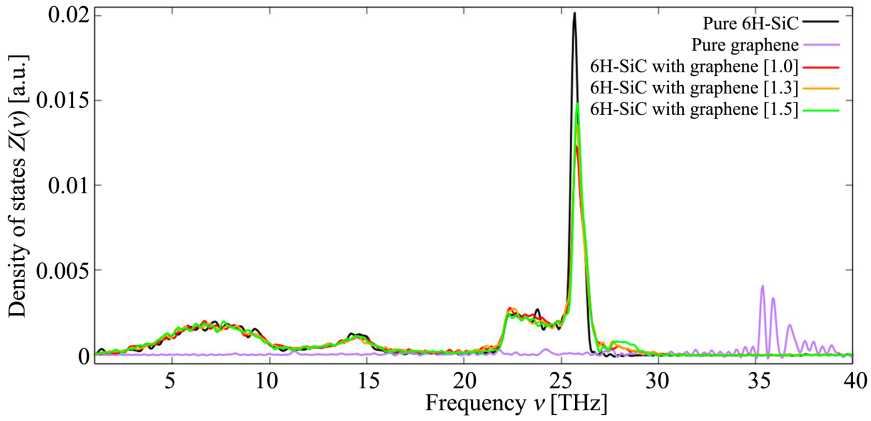

Figure 6. The spectrum of 6H-SiC for all equilibrated results, with the vibrational density of the states $Z(\nu)$ in arbitrary units plotted against the frequency ν in THz. The red/orange/green curves show the 6H-SiC structures which are grafted with graphene. The brackets contain the value in Ångström for the distance between the 6H-SiC crystal and the graphene layer.

total energies per atom, the 6H-SiC graphene structures tend to form more stable structural units than the 3C-SiC graphene structures (see **Table 1**). The 6H-SiC graphene with a distance of 1.0 Å proves to be the most stable structural unit here, which is due to the formation of additional bonds between the C-atoms of the graphene layer and the C-atoms of the surface of the 6H-SiC structure. Another difference is that after the large peak at around 25.7 THz for the three curves of the combined structures with graphene, there is no completely abrupt drop in the curves as in the case of pure SiC (black curve). In the lower part of the curves, a rather slow flattening can be seen up to approximately 30 THz, where even minor bumps are visible (especially for the distance of 1.5 Å). The formation of small shoulders at the high-frequency SiC-peaks causes the high-frequency peaks of graphene to disappear completely around 35 - 40 THz, which is due to interactions as well as bonds between the graphene and SiC.

Also, it can be seen here that the influence of the pure graphene (purple curve) as a graphene layer on the combined structures is once again only minimal. This can also be explained by the ratio of the lower number of atoms in the graphene layer to the 6H-SiC crystal. All in all, the curve for the pure graphene remains unchanged.

Next to the information on the structural properties, details on the spectral and dynamic behaviour give valuable insights into possible applications. The density of states is especially important for the understanding of thermodynamic properties, e.g. thermal heat transport.

4. Conclusions

If we consider the potential energies measured at the different distances between graphene and SiC crystals, we see that the most stable connection between a graphene layer and a 6H-SiC crystal is obtained at a distance of 1 Å.

The energetic situation also has influences on the structure, especially on the structure of the graphene layer. In the pair distribution functions we observe small shifts in C-C distances in the graphene layer from which we conclude that a change of hybridization in the graphene layer occurs. Again, this finding is best seen in the most stable combination at a distance of 1 Å between 6H-SiC and graphene. However, even in the 3C-SiC and also at moderate distances structural changes are seen. This leads to the conclusion that such a change of the electronic properties within the graphene layer may lead to interesting new applications.

From the spectra we may conclude that there is an influence from the graphene layer to the SiC-crystals both 6H-SiC and 3C-SiC, resp. The interactions between graphene and SiC reduce the height of the optical high-frequent peak at 25.7 THz in both crystal structures and as a consequence higher-frequent vibrations occur, since the number of vibrations is conserved. Again, this effect is more pronounced in 6H-SiC compared to 3C-SiC.

The structural changes and vibronic spectra are also used for the interpretation of thermodynamic properties such as thermal conduction. These properties correlate with the electronic transport properties.

Both types of structures graphene and the crystalline phases of SiC have mutual influences on structural and dynamic properties, and together with the impact on transport properties the combination of these structures may be used in (electro-) technical fields.

Conflicts of Interest

The authors declare no conflicts of interest regarding the publication of this paper.

References

[1] Ramsdell, L.S. (1947) Studies on Silicon Carbide. *American Mineralogist*, **32**, 64-82. https://pubs.geoscienceworld.org/msa/ammin/article-pdf/32/1-2/64/4243735/am-1947-64.pdf

[2] Powell, A. and Rowland, L. (2002) SiC Materials-Progress, Status, and Potential Roadblocks. *Proceedings of the IEEE*, **90**, 942-955. https://doi.org/10.1109/JPROC.2002.1021560

[3] Chiew, Y.L. and Cheong, K.Y. (2011) A Review on the Synthesis of SiC from Plant-Based Biomasses. *Materials Science and Engineering*: *B*, **176**, 951-964. https://doi.org/10.1016/j.mseb.2011.05.037

[4] Botsoa, J., Bluet, J.M., Lysenko, V., Marty, O., Barbier, D. and Guillot, G. (2007) Photoluminescence of 6h-SiC Nanostructures Fabricated by Electrochemical Etching. *Journal of Applied Physics*, **102**, Article ID: 083526. https://doi.org/10.1063/1.2798531

[5] Matsunami, H., Nishino, S., Odaka, M. and Tanaka, T. (1975) Epitxial Growth of α-SiC Layers by Chemical Vapor Deposition Technique. In: Cullen, G.W., Kaldis, E., Parker, R.L. and Rooymans, C.J.M., Eds., *Vapour Growth and Epitaxy*, Elsevier, Amsterdam, 72-75. https://doi.org/10.1016/B978-1-4831-9854-5.50014-8

[6] Li, J.-S., Wang, S.-C. and Hwang, C.-C. (2020) Preparation and High-Temperature Microwave Absorbing Properties of 6H-SiC/MWCNT/Silicon Resin Composites. *Materials Express*, **10**, 1-9. https://doi.org/10.1166/mex.2020.1612

[7] Zhokhov, A., Masalov, V., Matveev, D., Maksimuk, M., Zver'kova, I., Khasanov, S., Shmurak, S., Kiselev, A., Bazhenov, A. and Emelchenko, G. (2009) Synthesis of α-SiC Nanocrystals by Carbothermal Reduction of Spherical Nanoparticles of Amorphous Silicon Dioxide. *Physics of the Solid State*, **51**, 1723-1729. https://doi.org/10.1134/S1063783409080344

[8] Fan, J., Li, H., Wang, J. and Xiao, M. (2012) Fabrication and Photoluminescence of SiC Quantum Dots Stemming from 3C, 6H, and 4H Polytypes of Bulk SiC. *Applied Physics Letters*, **101**, Article ID: 131906. https://doi.org/10.1063/1.4755778

[9] Li, L., Xiao, G., Ding, P., Peng, Z., Chen, X., Li, Y., Nielsen, M. and Guo, L. (2021) Ultrafast All-Optical Switching in the Visible Spectrum with 6H Silicon Carbide. *ACS Photonics*, **8**, 2940-2946. https://doi.org/10.1021/acsphotonics.1c00605

[10] Sarikov, A., Marzegalli, A., Barbisan, L., Scalise, E., Montalenti, F. and Miglio, L. (2019) Molecular Dynamics Simulations of Extended Defects and Their Evolution in 3C-SiC by Different Potentials. *Modelling and Simulation in Materials Science and Engineering*, **28**, Article ID: 015002. https://doi.org/10.1088/1361-651X/ab50c7

[11] Bazylewski, P. and Fanchini, G. (2019) Graphene: Properties and Applications. In: Andrews, D.L., Lipson, R.H. and Nann, T., Eds., *Comprehensive Nanoscience and Nanotechnology*, Elsevier, Amsterdam, 87-304. https://doi.org/10.1016/B978-0-12-803581-8.10416-3

[12] Tiwari, S., Sahoo, S., Wang, N. and Huczko, A. (2020) Graphene Research and Their Outputs: Status and Prospect. *Journal of Science*: *Advanced Materials and Devices*, **5**, 10-29. https://doi.org/10.1016/j.jsamd.2020.01.006

[13] Novoselov, K., Falko, V.I., Colombo, L., Gellert, P.R., Schwab, M.G. and Kim, K. (2012) A Roadmap for Graphene. *Nature*, **490**, 192-200. https://doi.org/10.1038/nature11458

[14] Ye, R. and Tour, J.M. (2019) Graphene at Fifteen. *ACS Nano*, **13**, 10872-10878. https://doi.org/10.1021/acsnano.9b06778

[15] Avouris, P. and Dimitrakopoulos, C. (2012) Graphene: Synthesis and Applications. *Materials Today*, **15**, 86-97. https://doi.org/10.1016/S1369-7021(12)70044-5

[16] Hansen, J.-P. and McDonald, I.R. (2013) Theory of Simple Liquids. In: Hansen, J.-P. and McDonald, I.R., Eds., *Theory of Simple Liquids*, 4th Edition, Academic Press, Oxford, 1.

[17] Ciccotti, G., Frenkel, D. and McDonald, I.R. (1987) Simulation of Liquids and Solids. In: Ciccotti, G., Frenkel, D. and McDonald, I.R., Eds., *Simulation of Liquids and Solids*: *Molecular Dynamics and Monte Carlo Methods in Statistical Mechanics*, Amsterdam, New York, 1.

[18] Allen, M.P. und Tildesley, D.J. (1988) Computer Simulation of Liquids. 2nd Edition, Oxford University Press, Oxford.

[19] Garrison, B.J. (1992) Molecular Dynamics Simulations of Surface Chemical Reactions. *Chemical Society Reviews*, **21**, 155-162. https://doi.org/10.1039/cs9922100155

[20] Kumar, Y., Sahoo, S. and Chakraborty, A.K. (2021) Mechanical Properties of Graphene, Defective Graphene, Multilayer Graphene and SiC-Graphene Composites: A Molecular Dynamics Study. *Physica B Condensed Matter*, **620**, Article ID: 413250. https://doi.org/10.1016/j.physb.2021.413250

[21] Wang, Y.C., Zhu, Y.B., He, Z.Z. and Wu, H.A. (2020) Multiscale Investigations into

the Fracture Toughness of SiC/Graphene Composites: Atomistic Simulations and Crack-Bridging Model. *Ceramics International*, **46**, 29101-29110. https://doi.org/10.1016/j.ceramint.2020.08.082

[22] Tang, Y., Zhang, Z., Li, L., Guo, J. and Yang, P. (2022) Thermal Transport Enhancement Resolution for Graphene/Si and Graphene/SiC Interfaces. *International Journal of Thermal Sciences*, **171**, Article ID: 107231. https://doi.org/10.1016/j.ijthermalsci.2021.107231

[23] Yu, K., Zhao, W., Wu, X., Zhuang, J., Hu, X., Zhang, Q., Sun, J., Xu, T., Chai, Y., Ding, F. and Sun, L. (2018) *In Situ* Atomic-Scale Observation of Monolayer Graphene Growth from SiC. *Nano Research*, **11**, 2809-2820. https://doi.org/10.1007/s12274-017-1911-x

[24] Takamoto, S., Yamasaki, T., Nara, J., Ohno, T., Kaneta, C., Hatano, A. and Izumi, S. (2018) Atomistic Mechanism of Graphene Growth on a SiC Substrate: Large-Scale Molecular Dynamics Simulations Based on a New Charge-Transfer Bond-Order Type Potential. *Physical Review B*, **97**, Article ID: 125411. https://doi.org/10.1103/PhysRevB.97.125411

[25] Brenner, D.W. (1990) Empirical Potential for Hydrocarbons for Use in Simulating the Chemical Vapor Deposition of Diamond Films. *Physical Review B*, **42**, 9458-9471. https://doi.org/10.1103/PhysRevB.42.9458

[26] Liesegang, D. and Oligschleger, C. (2014) Spectral Modifications of Graphene Using Molecular Dynamics Simulations. *Journal of Modern Physics*, **5**, 149-156. https://doi.org/10.4236/jmp.2014.54025

[27] Beeman, D. and Alben, R. (1977) Vibrational Properties of Elemental Amorphous Semiconductors. *Advances in Physics*, **26**, 339-361. https://doi.org/10.1080/00018737700101403

[28] Oligschleger, C. and Schön, J. (1997) Calculation of Vibrational Properties of Selenium. *Journal of Physics*: *Condensed Matter*, **9**, 1049-1066. https://doi.org/10.1088/0953-8984/9/5/011

[29] Grzanka, E., Stelmakh, S., Gierlotka, S., Zhao, Y., Palosz, B. and Palosz, W. (2004) Examination of the Atomic Pair Distribution Function (PDF) of SiC Nanocrystals by *In-Situ* High Pressure Diffraction. *Journal of Alloys and Compounds*, **382**, 133-137. https://doi.org/10.1016/j.jallcom.2004.04.142

[30] Woznica, N., Hawelek, L., Fischer, H.E., Bobrinetskiy, I. and Burian, A. (2015) The Atomic Scale Structure of Graphene Powder Studied by Neutron and X-Ray Diffraction. *Journal of Applied Crystallography*, **48**, 1429-1436. https://doi.org/10.1107/S1600576715014053